ACS APPLIED MATERIALS & INTERFACES

Research Article

www.acsami.org

Effective Infiltration of Gel Polymer Electrolyte into Silicon-Coated Vertically Aligned Carbon Nanofibers as Anodes for Solid-State Lithium-Ion Batteries

Gaind P. Pandey,[†] Steven A. Klankowski,[†] Yonghui Li,[‡] Xiuzhi Susan Sun,[‡] Judy Wu,[§] Ronald A. Rojeski,[∥] and Jun Li*[,†]

[†]Department of Chemistry, Kansas State University, Manhattan, Kansas 66506, United States

[‡]Department of Grain Science and Industry, Kansas State University, Manhattan, Kansas 66502, United States

[§]Department of Physics and Astronomy, University of Kansas, Lawrence, Kansas 66045, United States

[∥]Catalyst Power Technologies, 200 Carlyn Avenue, Suite C, Campbell, California 95008, United States

Supporting Information

ABSTRACT: This study demonstrates the full infiltration of gel polymer electrolyte into silicon-coated vertically aligned carbon nanofibers (Si-VACNFs), a high-capacity 3D nanostructured anode, and the electrochemical characterization of its properties as an effective electrolyte/separator for future all-solid-state lithium-ion batteries. Two fabrication methods have been employed to form a stable interface between the gel polymer electrolyte and the Si-VACNF anode. In the first method, the drop-casted gel polymer electrolyte is able to fully infiltrate into the open space between the vertically aligned core−shell nanofibers and encapsulate/stabilize each individual nanofiber in the polymer matrix. The 3D nanostructured Si-VACNF anode shows a very high capacity of 3450 mAh g^{-1} at C/10.5 (or 0.36 A g^{-1}) rate and 1732 mAh g^{-1} at 1C (or 3.8 A g^{-1}) rate. In the second method, a preformed gel electrolyte film is sandwiched between an Si-VACNF electrode and a Li foil to form a half-cell. Most of the vertical core−shell nanofibers of the Si-VACNF anode are able to penetrate into the gel polymer film while retaining their structural integrity. The slightly lower capacity of 2800 mAh g^{-1} at C/11 rate and ∼1070 mAh g^{-1} at C/1.5 (or 2.6 A g^{-1}) rate have been obtained, with almost no capacity fade for up to 100 cycles. Electrochemical impedance spectroscopy does not show noticeable changes after 110 cycles, further revealing the stable interface between the gel polymer electrolyte and the Si-VACNFs anode. These results show that the infiltrated flexible gel polymer electrolyte can effectively accommodate the stress/strain of the Si shell due to the large volume expansion/contraction during the charge−discharge processes, which is particularly useful for developing future flexible solid-state lithium-ion batteries incorporating Si-anodes.

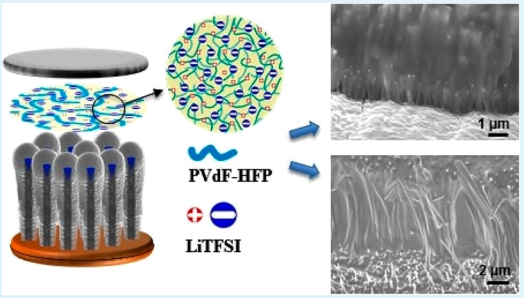

KEYWORDS: *3D silicon anodes, gel polymer electrolyte, solid-state lithium ion battery, silicon-coated vertically aligned carbon nanofibers, polymer infiltration, electrochemical impedance spectroscopy*

INTRODUCTION

Lithium-ion batteries (LIBs) are widely used for powering today's portable electronics, and development is underway for supporting future hybrid electric vehicles.[1,2] The emerging markets of electric vehicles (EVs) demand LIBs with higher energy and power densities as well as long cycle life.[1] While extensive research efforts have been placed on developing high-energy and high-power electrode materials, the increasing attention toward safety and the hazards of flammable organic solvents used in commercial LIBs has directed research focusing on components with better safety and stability properties.[3] The development of solid-state batteries that employ polymer electrolytes may be a viable solution.[4] Solid polymer electrolytes (SPEs) have shown great potential to suppress the risks of thermal runaway in Li-ion or Li batteries.[2,4−6] However, the limited ionic conductivity (10^{-5}–10^{-6} S cm^{-1} at ambient temperatures), difficulties in infiltrating into electrodes, and high interfacial resistance due to poor contact and wetting of SPEs on common composite electrodes prevented their implementation at the device level.[4−6] To obtain a good rate capability, long-term stability and cycling ability, alternative polymer electrolyte should possess high ionic conductivity along with sufficient cationic diffusion and stable electrode/electrolyte interfaces to achieve fast charge−discharge and long cycle life.[3] Within this context, gel polymer electrolytes (GPEs) have been considered as promising alternative to SPEs.[4] GPEs using polymer network as matrix to immobilize the liquid components have higher ionic

Received: July 16, 2015
Accepted: September 1, 2015
Published: September 1, 2015

DOI: 10.1021/acsami.5b06444
ACS Appl. Mater. Interfaces 2015, 7, 20909−20918

conductivity than that of intrinsic SPEs and higher stability than electrolyte solutions. Various polymer materials such as poly(methyl methacrylate) (PMMA),[7,8] poly(vinylidene fluoride-hexafluoropropylene) (PVdF-HFP),[8,9] and so on have been applied as polymer matrix in GPEs for LIBs.

The development of high capacity anode to replace carbon-based materials, commonly used for commercial LIBs, is another active research area for high-performance LIBs. Li-alloying anodes (Si, Sn, Ge, etc.) have much higher Li storage capacity than commercial carbon-based anodes (372 mAh g^{-1}).[10−15] Among them, Silicon (Si) has been identified as one of the best candidates. Si has a high theoretical specific capacity of 4200 mAh g^{-1}, a very low lithiation potential <0.5 V vs Li/Li^+, and is naturally abundant and environmentally benign.[12,16] Moreover, Si also has a large volumetric capacity of 8322 mAh cm^{-3}.[17,18] In the amorphous state, Si has a maximum obtainable capacity of ∼3800 mAh g^{-1} at room temperature, which is ten times higher than that of conventional graphite anodes.[16] However, Li−Si alloying during charging causes up to 320% volume expansion in the anode and hence induces severe anisotropic stress, leading to particle pulverization, solid electrolyte interphase (SEI) destabilization, and consequently fast capacity fading in only tens of cycles.[16,19] Various nanostructured Si materials including nanoparticles, nanowires, hollow spheres, egg yolk, etc. have been prepared to reduce the internal stress and to make use of their large specific surface area and short Li^+ diffusion length in solids.[10,20−22] Hybrid core−shell nanofibers utilizing a highly conductive and stable nanofiber core to support a coaxial Si shell has also been demonstrated with the capability to further improve the power rate while maintaining the high capacity and good cycle stability.[23−27]

It is of great interest to combine the GPEs with high-performance 3D nanostructured Si anodes, particularly for the development of flexible thin-film batteries.[28] However, the progress in this area is hindered so far by the persistent challenges in infiltrating polymer electrolytes into the interior surface of the 3D nanostructured electrodes and maintaining good electrical contact between polymer electrolytes and the surface of active Si materials during charge−discharge.[28,29] To address these problems, several attempts have been made with two efforts: (1) using the fluidic characteristics of GPEs at their initial liquid states to form good contact with the electrodes and (2) using vertical 3D Si electrodes to allow easier electrolyte access. Kil et al. demonstrated highly ion-conductive, bendable polymer electrolytes that are conformable to a 40 nm Si thin film coated on an array of Cu micropillars (18 μm in height and ∼153 μm in diameter).[29] However, the cycling performance of the half-cell (Si anode/gel electrolyte/Li) was poor, and the extract capacity quickly decreased from ∼1100 mAh g^{-1} (relative to Si mass) in the second cycle to ∼650 mAh g^{-1} in the 10th cycle. Vlad et al. demonstrated that GPE can even effectively infiltrate into the space between vertically aligned Si nanowires to form a composite membrane with a more meaningful Si mass loading that can be peeled off from the supporting Si substrate.[30] A properly connected half-cell demonstrated a relatively high specific capacity of ∼2000 mAh g^{-1} (relative to Si mass) at C/20 rate with little capacity decay over 50 cycles, but dropping to ∼1000 mAh g^{-1} at 1C rate.[30] They further built a flexible roll-up full battery by casting $LiCoO_2$ slurry on such free-standing Si nanowire-embedded GPE membrane as the anode.

Recently, we reported that high specific capacity over ∼3000 mAh g^{-1} at 1C over 500 cycles can be obtained in volatile conventional liquid electrolyte with a Si LIB anode in a unique vertical 3D architecture, i.e., a nanostructured coaxial Si shell coated on vertically aligned carbon nanofibers (VACNFs).[31,32] This vertical 3D architecture was fabricated on a Cu foil and can be flexibly bended without structural degradation. In this study, this Si-coated VACNF anode is coupled with a self-standing, bendable, solid-like, flexible GPE and characterized toward the development of flexible solid-state LIBs. The employed GPE has a high conductivity of ∼2.2 × 10^{-3} S cm^{-1}, sufficient cationic transference number, and good thermal and mechanical stabilities, which can infiltrate into the high-capacity 3D-nanostructured silicon anode to form a stable electrode−electrolyte interface. The infiltrated gel electrolyte is able to effectively accommodate the stress/strain due to the very large Si volume change (up to 400%) during charge−discharge which has been a critical limiting factor for Si anodes. The Si-VACNFs electrodes show high specific capacity, good rate performance, and long cycling stability in such a solid-like, flexible GPE.

EXPERIMENTAL SECTION

Preparation of Gel Polymer Electrolyte. The copolymer, poly(vinylidene fluoride-hexafluoropropylene) (PVdF-HFP; MW ≈ 400 000), ethylene carbonate (EC, > 99%), dimethyl carbonate (DMC, anhydrous, > 99%), and lithium bis(trifluoromethane) sulfonimide (LiTFSI, 99.95%) were obtained from Sigma-Aldrich and used without further purification. The intermediate solvent tetrahydrofuran (THF, analytical grade) was purchased from Fisher Scientific, U.S.A. The electrolyte solution was prepared by dissolving LiTFSI in the binary solvent system of EC and DMC, where the salt concentration and mixing ratio of EC and DMC were kept 1.0 M salt and 1:1 (w/w) of EC/DMC, respectively. The gel polymer electrolyte was prepared by a solution casting method.[33] The host polymer PVdF-HFP was separately dissolved in THF by magnetic stirring at ∼60 °C and an appropriate amount of liquid electrolyte was mixed in this solution. The resulting mixture was stirred for 12 h to form homogeneous solution and then poured into glass Petri dishes and allowed the intermediate solvent, THF, to evaporate to obtain a self-standing solid, flexible, gel electrolyte film of thickness ∼0.3 mm (Figure 1, parts a and b). The mass ratio of polymer to the LiTFSI solution was about 1:6 in the resulting gel used to characterize Si-coated VACNFs anode. The gel electrolyte films of other ratios (1:3, 1:4, and 1:5) were also prepared to measure conductivity and Li^+ transport number for comparison. The viscous solution of gel polymer electrolyte (in THF) was also used to fabricate cells with Si-coated VACNFs anodes. The whole preparation process was performed in an argon-filled glovebox (MBraun LabStar50, Stratham, NH, U.S.A.).

VACNF Growth and Si Sputtering. Pure copper foils (84 μm, Copper 102, Hamilton Precision Metals, PA) were coated with a 300 nm thick chromium layer, followed by a 30 nm nickel catalyst layer using a high-vacuum PerkinElmer 4400 series magnetron sputtering system at the UHV Sputtering Inc. (Morgan Hill, CA). The Cr/Ni coated Cu sheets were then cut into ∼18 mm diameter disks for VACNFs growth using a DC-biased plasma enhanced chemical vapor deposition (PECVD) system (AIXTRON, CA) following a procedure reported in the literature.[34−36] First, a pretreatment procedure was applied by thermally heating the substrate to 500 °C in 250 sccm NH_3 at a pressure of 3.9 Torr, followed with a 40 W plasma treatment for 60 s. The combined effects of thermal dewetting and NH_3 plasma etching broke down the Ni film into randomly distributed nanoparticles that catalyzed the growth of VACNFs in a tip growth mode.[34,35] The diameter and areal density of the VACNFs were determined by these Ni nanoparticles. Following the pretreatment, a mixture of acetylene and NH_3 was introduced as the precursor at 750 °C and a pressure of 4.6 Torr. The NH_3 flow was controlled at a rate of 250 sccm, and the acetylene was operated at 70 sccm for this

DOI: 10.1021/acsami.5b06444
ACS Appl. Mater. Interfaces 2015, 7, 20909−20918

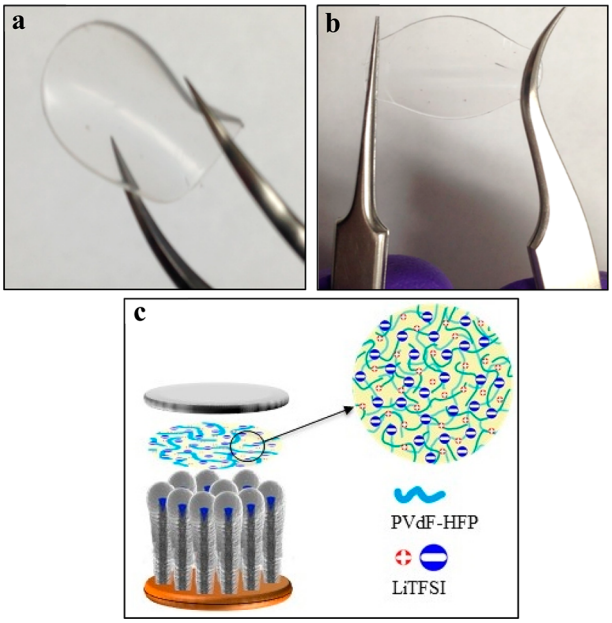

Figure 1. (a, b) Optical images of the flexible gel polymer electrolyte film with good mechanical stability that can be easily bent or stretched. (c) Schematic illustration of the Si-VACNF half-cell with the gel electrolyte film.

experiment. The plasma power was kept at 45 W for 30 min to grow ~5.0 μm long VACNFs. VACNFs have an average diameter of 150 nm and an areal density of ~1.1 × 10^9 CNFs cm^{-2}. Pure silicon (Si) was deposited on VACNFs to form the VACNF-Si core−shell nanowire arrays by high vacuum magnetron sputtering under a processing pressure of ~8 mTorr (adjusted with a flux of ultrapure argon) at a deposition rate of 30 nm per min in two different thickness at UHV Sputtering Inc. The nominal thicknesses of Si (equivalent to the film thickness on a flat surface) were measured as ~0.456 and 1.50 μm in situ, respectively, using a quartz crystal microbalance (QCM) and validated by scanning electron microscopy (SEM) measurements of a silicon wafer placed beside the Cu substrate.[31]

Cell Assembly and Electrochemical Measurements. To evaluate the electrochemical performance of the VACNF-Si core−shell nanowire array anode (two different Si thickness) with gel polymer electrolyte, half cells were assembled into stainless steel coin cells (CR2032-type) in a glovebox containing less than 0.5 ppm of H_2O or O_2. The gel electrolyte was incorporated with two different processes. In the first process, the viscous solution of gel polymer electrolyte (in THF) was drop-casted over Si-coated VACNF anodes and then allowed THF to evaporate completely. After 2−3 layers of electrolyte coating, the anode was placed in the coin cell case, and an Li-disc (16 mm, as counter and reference electrode) was placed over it to complete the cell assembly. In the second process, the coin cell was fabricated by sandwiching a solid, flexible, self-standing gel film (punched into 18 mm diameter) between an Si-coated VACNF electrode and an Li-disc (Figure 1c).

Galvanostatic charge−discharge cycling was performed at room temperature and operated at voltages of 0.05−1.5 V versus Li/Li^+ using an MTI 8 channel battery analyzer (MTI Corporation, Richmond, CA). The gravimetric capacity was calculated by dividing only the mass of Si over the electrode surface, which was calculated from the nominal thickness (0.456 and 1.50 μm) measured by SEM at the cleaved cross-section of a reference Si wafer and the density of sputtered silicon (2.33 g cm^{-3}). In a previous report,[31] it was demonstrated that the total Li^+ storage capacity of Si-coated VACNFs with 500 nm nominal Si thickness is about 10 times of that of bare VACNFs. In addition, the low potential limit for Li insertion cycle was increased from 0.001 to 0.05 V which further reduce the Li intercalation into VACNF core. Therefore, in such core−shell structure, >95% of the capacity was from the active Si-shell and, hence, the capacity was calculated by taking only the mass of silicon. It also provides a direct comparison with literature for better understanding whether the full theoretical capacity of Si has been utilized. Cyclic voltammetry (CV) was performed in the potential range of 0.05−1.5 V versus Li/Li^+ at different scan rates 0.1, 0.25, and 1 mV s^{-1} (three cycles at each rate) after initial 4 charge−discharge cycles (2 cycles at 37.5 μA cm^{-2}, and 2 cycles at 75 μA cm^{-2}). AC impedance spectroscopy was performed using a CHI 760D electrochemical workstation with a 10 mV AC potential over a frequency range from 100 kHz to 0.01 Hz at different insertion potential (0.55 to 0.05 V versus Li/Li^+). Both the as-prepared electrodes and those disassembled from the coin-cells after half-cell tests were stored and transferred in air before inspection with SEM (FEI Nova NanoSEM 430, 3.5 kV).

RESULTS AND DISCUSSION

Gel Electrolyte: Conductivity, Stability Window and Li-Ion Transference Number. As described in the Experimental Section, the PVdF-HFP based membranes were swollen with an organic electrolyte made of a solution of LiTFSI in EC/DMC. The primary goal is to prepare a GPE film in such a composition that it can be used as electrolyte and separator to characterize the Si-coated VACNF core−shell nanowire array electrodes while maintaining vertically aligned structure during cell operation. The copolymer PVdF-HFP can retain a high amount of liquid electrolyte (up to 1:6 ratio) while displaying highly flexible, stretchable, self-standing, nonbrittle GPE film with the desired mechanical stability, which is an important requirement for their application as electrolyte/separator in nanostructured 3D LIBs. Figure 1, parts a and b, shows two representative photographs of the GPE films, demonstrating their transparent, self-standing, stretchable properties.

For the applications as an electrolyte/separator in LIBs, the gel film needs to have a high ionic conductivity, which strongly depends on the polymer to liquid electrolyte ratio. Therefore, the conductivity of the GPE is first investigated as a function of the polymer and liquid electrolyte fraction. It can be seen from Table 1 that the conductivity increases with increasing content

Table 1. Room Temperature Conductivity and Li-Ion Transference Number for Different Compositions of Gel Polymer Electrolytes

gel electrolyte composition: PVdF-HFP: 1 M LiTFSI in EC/DMC (w/w)	conductivity (S cm^{-1})	Li-ion transport number (T_{Li^+})
1:3	1.4 × 10^{-4}	
1:4	6.4 × 10^{-4}	0.46
1:5	1.6 × 10^{-3}	0.45
1:6	2.2 × 10^{-3}	0.41

of liquid electrolyte, and a conductivity of ~2.2 × 10^{-3} S cm^{-1} can be achieved for the gel film consisting of 1:6 polymer to liquid electrolyte weight ratio. The increase of conductivity with the liquid electrolyte content can be explained by the higher salt concentration in the gel film and higher amount of solvent molecules (EC and DMC), which allow a higher mobility of Li^+ ions.

Figure 2a shows the temperature dependence of the electrical conductivity of the gel polymer electrolyte (1:6 ratio) in the temperature range from 60 to −40 °C in the first three heating/cooling cycles. For the first heating cycle (marked as 1 in Figure

DOI: 10.1021/acsami.5b06444
ACS Appl. Mater. Interfaces 2015, 7, 20909−20918

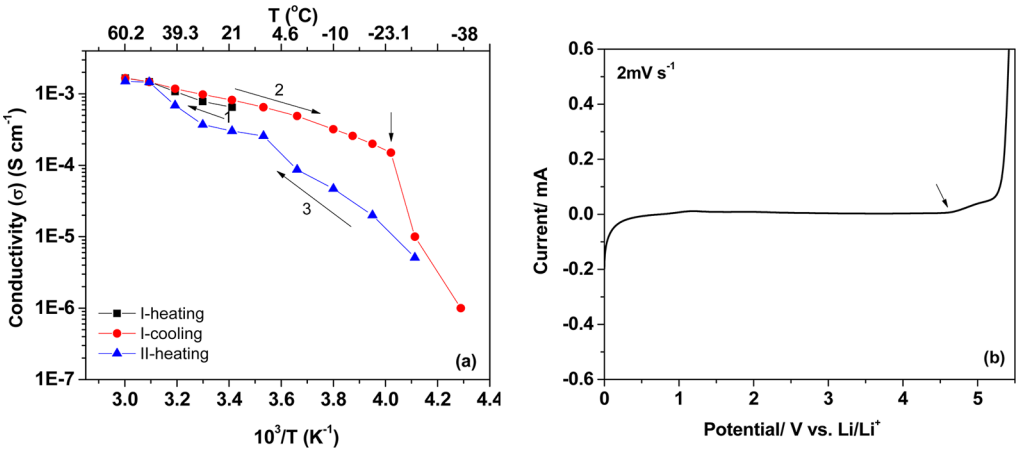

Figure 2. (a) The "Conductivity vs $1/T$" plot of the gel polymer electrolyte film (1:6 ratio) for the first three heating/cooling steps. (b) Linear sweep voltammetry curve of a cell: SS |gel polymer electrolyte | Li at the scan rate of 2 mV s^{-1}. Working electrode: Stainless steel disk. Reference and counter electrode: Li foil.

2a), the conductivity increases slightly in the temperature range of 20 to 60 °C, while the conductivity in the cooling cycle (marked as 2 in Figure 2a) first slowly decreases as the temperature is lowered from 60 °C to −25 °C and then suddenly drops by several orders of magnitude as the temperature goes below −25 °C, which confirms that solvent molecules (EC and DMC) in the polymer matrix were frozen completely. In the heating cycle from −40 °C, the gel film shows almost 1 order of magnitude less conductivity than in the cooling cycle, which quickly increases at above room temperature and matches the value in the first heating cycle at around 50 °C. This conductivity measurement shows that the gel can be used in the temperature range between 60 to −20 °C. In this temperature range, the log σ vs $1/T$ plot shows a nonlinear behavior (first cooling in Figure 2), which follows the non-Arrhenius Vogel-Tammen-Fulcher (VTF) equation:

$$\sigma(T) = AT^{-1/2} \exp\left(\frac{-B}{T - T_0}\right) \quad (1)$$

where, A is the pre-exponential factor, T_0 is the equilibrium glass transition temperature which is usually close to the T_g values, and B is a pseudoactivation energy which is associated with the critical free volume for the charge-carriers motion. VTF eq 1 is a phenomenological way to interpret ion transport data in amorphous polymer electrolyte above the glass transition.[37] The temperature dependent on conductivity measurement shows that gel electrolyte exhibits ionic conductivity of ∼3 × 10^{-3} S cm^{-1} at 60 °C and ∼2 × 10^{-4} S cm^{-1} at −20 °C, defining the applicable temperature range in the LIBs. Figure 2b shows the linear sweep voltammetry curve of the GPE of 1:6 ratio. The potential of the working electrode was scanned at 2 mV s^{-1} from 0 to 5.5 V vs Li/Li^+. The electrolyte is clearly stable up to 4.7 V, which is acceptable for high voltage LIB applications. Only a small reduction current is observed at 0, likely due to electroplating of Li. Setting the low potential limit at 0.05 V can largely avoid this.

The differential scanning calorimetry (DSC) and thermogravimetric analysis (TGA) curves of PVdF-HFP/EC-DMC-LiTFSI (1:6) GPE are shown in Figure S1. The two endothermic peaks at ∼5 and 114 °C are related to the melting point of the entrapped liquid electrolyte and crystalline part of the PVdF-HFP, respectively. The melting temperature of the PVdF-HFP in the gel electrolyte is much lower than pure PVDF-HFP (∼145 °C) and also the peak becomes relatively broader indicating the amorphous nature of the gel electrolyte film due to presence of a large amount of liquid electrolyte. The amorphous phase is favorable to increasing the ionic conductivity.[5] The TGA curve (Figure S1b) shows only ∼3% weight loss at 100 °C which indicates that the evaporation rate of entrapped liquid electrolyte in the PVdF-HFP matrix is very slow. The high retention ability of this gel electrolyte is critical to ensure the higher safety of LIBs compared to the volatile organic liquid electrolyte.

Li-ion transference number (T_{Li}^+) is a key parameter to optimize the performance of polymer electrolyte for LIBs. In fact, high T_{Li}^+ is required for high powder density. The T_{Li}^+ of the GPE is investigated by the combination of dc polarization and ac impedance spectroscopy, as described in the Supporting Information (SI). Figure S2 shows the chronoamperometric and impedance measurement for PVdF-HFP/EC-DMC-LiTFSI (1:6) gel electrolyte. The T_{Li}^+ was calculated using eq (2) of SI and presented in Table 1. The T_{Li}^+ of PVdF-HFP/EC-DMC-LiTFSI (1:6) gel electrolyte is 0.41, which is used to fabricate half-cells in later studies. The T_{Li}^+ value increases slightly for gel electrolyte film with higher polymer contents since ions tend to form ion pairs at higher liquid electrolyte composition, which increases the ion size and hence decreases their transfer velocity.[38] Nevertheless, higher liquid electrolyte composition is selected for use as electrolyte/separator due to its good mechanical strength and flexibility. Moreover, the T_{Li}^+ of this GPE is comparable to the organic liquid electrolyte and other PVdF-HFP based electrolytes.[39,40]

Microscopic Characterization of Si-Coated VACNF Anode. Figures 3, parts a and b, and S3 show the SEM images of an as-grown VACNF array on a Cu foil and Si-coated VACNF array with thickness 0.5 and 1.5 μm, respectively. The CNFs are firmly attached to the Cu foil substrates, providing a highly conductive electron pathway between the active Si shell and the current collector.[32] The conductivity of CNFs is ∼2.5 × 10^3 S cm^{-1}. After sputter-coating of the Si layer, the individual CNFs show a cotton swab appearance with a larger mass at the tip that tapers gradually down the CNFs. SEM images indicate that Si form coaxial shells with larger radical thickness at the fibers tips and gradually thinned moving down to the base. The largest average outer diameter is ∼450 nm,

DOI: 10.1021/acsami.5b06444
ACS Appl. Mater. Interfaces 2015, 7, 20909−20918

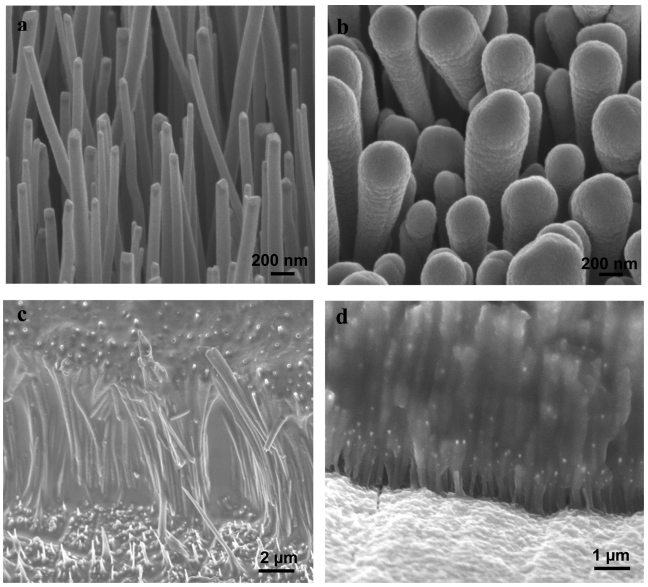

Figure 3. SEM images of (a) an as-grown VACNF array with an average length of 5 μm, (b) a similar VACNF array after sputter-coating with silicon at a nominal thickness of 0.5 μm, (c) and (d) the Si-coated VACNF electrodes after half-cells charge−discharge cycles. The half-cells were fabricated by (c) sandwiching a solid gel electrolyte film and (d) drop-casting the liquid polymer electrolyte over Si-VACNF electrode and then drying it. Panels (a) and (b) are 45° perspective views, and panels (c) and (d) are the cross-sectional view.

appearing near the fiber tips (Figures 3b and S3b). More thorough characterization with the cross-sectional FESEM and TEM images of the Si-coated VACNFs scraped off from the surface can be found in our previous publications.[31,32,41] A rough texture extends across the shell surface, representing a distinctive feature of the nanocolumnar microstructure that commonly formed in thick sputtered films.[32,42] The detailed structural characterization of Si-coated VACNF anode is described in our previous publications.[31,32,41] The nanocolumnar structure of Si-coated VACNFs facilitates the electrolyte penetration into the Si shell and also increases the active electrochemical surface area of the anode for fast Li-ion diffusion, which helps to reduce the polarization during cycling. In the 1.5 μm thick Si-coated VACNFs, the open space between the CNFs is reduced significantly with respect to the thinner Si coating, as shown in Figure S3(d−f). As a result, the gel electrolyte is not able to access the entire Si shell, leading to slightly lower specific capacity than the thinner Si coating as will be shown in later sections.

Figures 3, parts c and d, and S4 depict SEM images of the electrodes disassembled after half-cell tests from the coin-cells. The upper surface of the GPE film is smooth and only a few longer CNFs tips stick out, indicating that the nearly all VACNFs are embedded in the gel polymer electrolyte. The cross-sectional view of the cut electrode (Figures 3c and S4b) confirms that even the preformed GPE film, originally sandwiched between Li metal and Si-VACNFs electrode, was able to infiltrate into the Si-VACNF anode. The 3D electrode structure remained stable during both cell assembly and electrochemical characterization. Besides, the filled GPE also enhances the mechanical tolerance of the Si shell against volumetric changes during cycling. Alternatively, the GPE was directly drop-casted over a Si-coated VACNFs array when it was still in the initial liquid state. As shown in Figures 3d and S4 (c and d), the GPE was able to fill in the open space between VACNFs and the vertically aligned 3D structure of the Si-VACNFs anode remained intact after complete evaporation of THF and during cycling.

Electrochemical Characterization. Figures 4 and S5 show the cyclic voltammograms of a representative half-cell

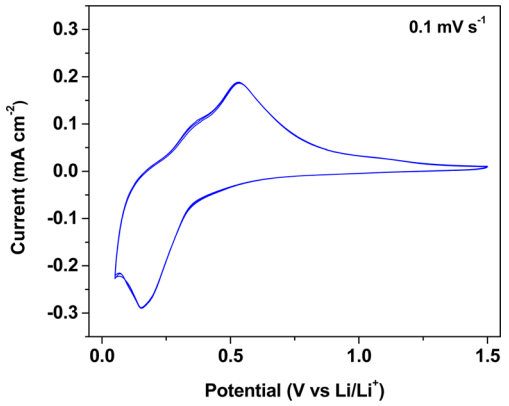

Figure 4. Cyclic voltammogram of a Si-VACNF electrode (Si thickness of 0.5 μm) in the gel electrolyte between 1.5 to 0.05 V (vs Li/Li^+) at the scan rate of 0.10 mV s^{-1} (three cycles). The measurements are made after 4 initialization charge−discharge cycles (2 cycles at 37.5 μA cm^{-2} and 2 cycles at 75 μA cm^{-2}).

made of Si-coated VACNF anode and the GPE at different scan rates. In the cathodic scan, the formation of the Li−Si alloy began at a potential ~0.33 V, and the cathodic current reaches a maximum at ~0.15 V, indicating the largest Li insertion. Since the CV was recorded after the initial 4 stabilization charge−discharge cycles, the Si shell was already converted into metastable amorphous structure (Li−Si) without forming intermediate crystalline phases.[42] In the anodic scan, two delithiation peaks at ~0.35 and ~0.53 V are observed, which is typical for amorphous Si anodes.[10,31,43] At higher scan rates (Figure S5), the formation of the Li−Si alloy began at the same potential (~0.33 V) and became quite large below 0.1 V. Upon delithiation, peak slightly shifts toward higher potential and became broader. The CV characteristics were consistent with the reported literature of Si anodes in organic liquid electrolytes.[10,13,44]

The voltage profiles of the Si-VACNFs/GPE half-cell in the first and second galvanostatic cycles at the C/21 rate as well as the sixth and twelfth cycles at C/10.5 rate are shown in Figure 5a. The specific capacity was calculated using the mass of coated Si. To make consistent comparison, all referred C-rates are based on the theoretical specific capacity of amorphous Si ≈ 3800 mAh g^{-1} rather than using the actual charge−discharge time which varies with the conditions and history of cell operations. In the first cycle, the insertion and extraction capacities reached 4743 and 3618 mAh g^{-1}, respectively, and the Coulombic efficiency is only 76%. The low efficiency for the first cycle can be mainly due to the excess reaction in the Li insertion process associated with the formation of an irreversible SEI layer at the Si surface,[45] reactions of Li with SiO_x impurities present on the Si surface ($SiO_x + 2xLi \rightarrow Si + xLi_2O$), and other irreversible side reactions, which is common in Si anodes.[31] In addition, the first insertion curve displayed a short step at about 0.82 V and a long plateau below 0.35 V, confirming the SEI formation similar to that in the case of Si/organic electrolyte.[46] However, the second cycle showed

DOI: 10.1021/acsami.5b06444
ACS Appl. Mater. Interfaces 2015, 7, 20909−20918

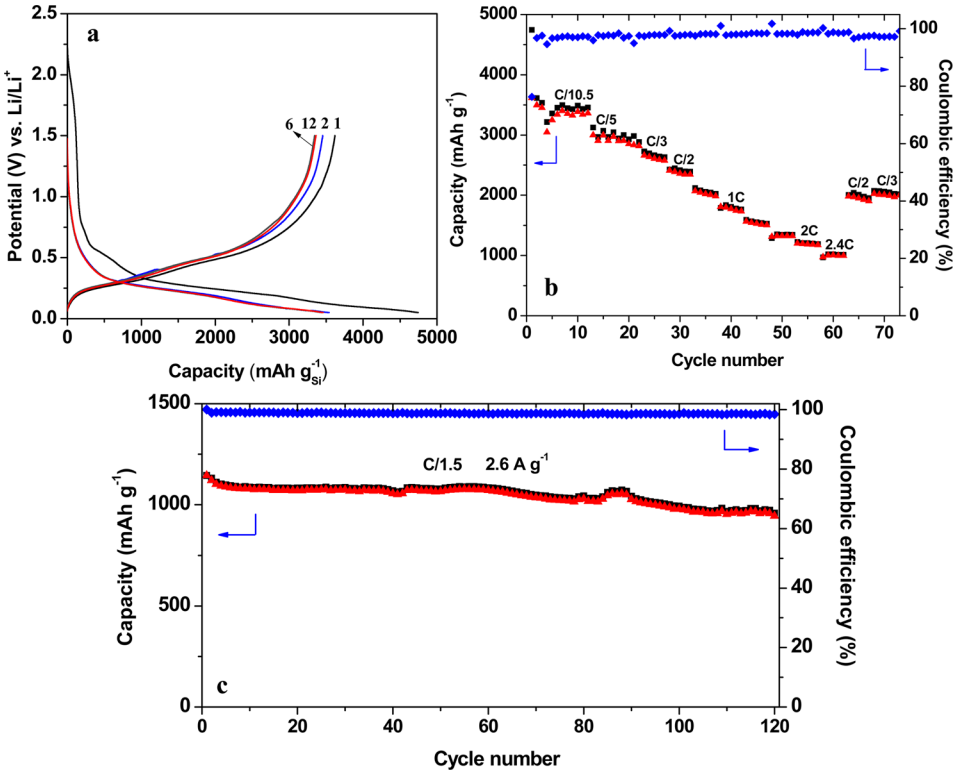

Figure 5. (a) The voltage profiles of the 1, 2, 6 and 12th galvanostatic charge and discharge cycles of the half-cell: Li | drop-casted gel electrolyte | Si-VACNFs (Si ≈ 0.5 μm), at the C/21 (1 and 2) and C/10.5 (6 to 12) rates (C rate is calculated based on the theoretical capacity of amorphous Si ≈ 3800 mAh g^{-1}). (b) The rate performance of the half-cell: Li | drop-casted gel electrolyte | Si-VACNFs, at various rates from C/10.5 (0.36 A g^{-1}) to 2.4C (9.2 A g^{-1}). (c) Cycling performance of the Si-VACNFs (Si ≈ 0.5 μm) electrode with a sandwiched gel polymer electrolyte film at C/1.5 rate (current density of 2.6 A g^{-1}) between 0.05 to 1.5 V (black ■: lithium insertion into Si-VACNFs; red ▲: lithium extraction from Si-VACNFs; blue ♦: Coulombic efficiency.

insertion and extraction capacities of 3536 and 3452 mAh g^{-1}, respectively, with Coulombic efficiency jumping up to ~97.6%. After initial 4 cycles, the capacities stabilize at ~3450 mAh g^{-1} at C/10.5 rate with the Coulombic efficiency >98% in subsequent cycles. The capacity loss in the initial cycles is partially attributed to the conversion of the crystalline Si coating with a higher theoretical capacity (~4200 mAh g^{-1}) into amorphous Si with a lower capacity (~3800 mAh g^{-1}).[16] In the later cycles, the lithium insertion shows a sloping profile between 0.25 and 0.05 V which is consistent with the behavior of amorphous silicon.[47,48]

After the initial stabilization cycles, the rate performance of Si-coated VACNFs electrode with gel polymer electrolyte was evaluated by galvanostatic charge−discharge at different currents from C/10.5 (0.360 A g^{-1}) to as high as 2.4 C (9.20 A g^{-1}), each for five cycles. Figures 5b and S6a show the insertion/extraction capacities versus the cycle number and voltage profiles at different rates, respectively. The extraction capacities based on the Si mass are 3342.8, 2588.2, 2342, 1732.8, and 1006.1 mAh g^{-1}, derived from the last cycle at C/10.5, C/3, C/2, 1C and 2.4C, respectively. The capacities at each rate were almost stable with very small fading. Thus, the Si-coated VACNFs anode with solid-like GPE has shown a high reversibility and good capacity retention. It is noted that these results clearly surpassed the specific capacity of ~2000 mAh g^{-1} at C/20 rate and ~1000 mAh g^{-1} at 1C rate reported in the state-of-the-art flexible battery study with GPE infiltrated into vertically aligned Si nanowires.[30]

The high rate was known to cause electrode degradation and thus when the rate was changed from 2.4C back to C/2, the capacity was found to drop from 2342 mAh g^{-1} to 1926 mAh g^{-1}. After the rate test, the same cell was cycled at C/3 (1.28 A g^{-1}) rate for 150 cycles (Figure S6b). The cell retained a capacity of >810 mAh g^{-1} after 225 overall cycles, which is still more than two times larger than that of graphite. To examine the long-term cycling stability, another half-cell fabricated by sandwiching a GPE film between a Si-VACNFs (Si ~ 0.5 μm) anode and a Li metal was charge−discharged at a high rate of 2.6 A g^{-1} (or C/1.5 rate) for more than 100 cycles (Figure 5c) after 4 initialization cycles at C/21 rate. The capacity retention of the cell is ~88% from fifth to 100th cycle with Coulombic efficiency ~99%. Even at the high current density of 2.6 A g^{-1} (or C/1.5 rate), the solid-state half-cell was able to maintain a capacity ~1050 mAh g^{-1}.

The 1.5 μm thick Si-coated VACNFs anode were also characterized using the GPE. Figures S7a and S7b illustrate the rate performance and voltage profiles at different rates, respectively, for such a half-cell. The extraction capacities based on the Si mass were 2517.6, 1969.3, 1280.9, and 1003.1 mAh g^{-1} derived from the last cycle at C/13, C/5, C/2.4 and C/1.8, respectively. After the rate performance, the cell was cycled at C/4 rate until 200 cycles (Figure S7c). After 200 cycles, the capacity remained >570 mAh g^{-1}. The thick Si-coated VACNFs anode showed less specific capacities, particularly at higher rates, which is most likely due to two reasons: (i) the 1.5 μm Si-coating on VACNFs present less open volume between fibers compared to 0.5 μm Si-coating

DOI: 10.1021/acsami.5b06444
ACS Appl. Mater. Interfaces 2015, 7, 20909−20918

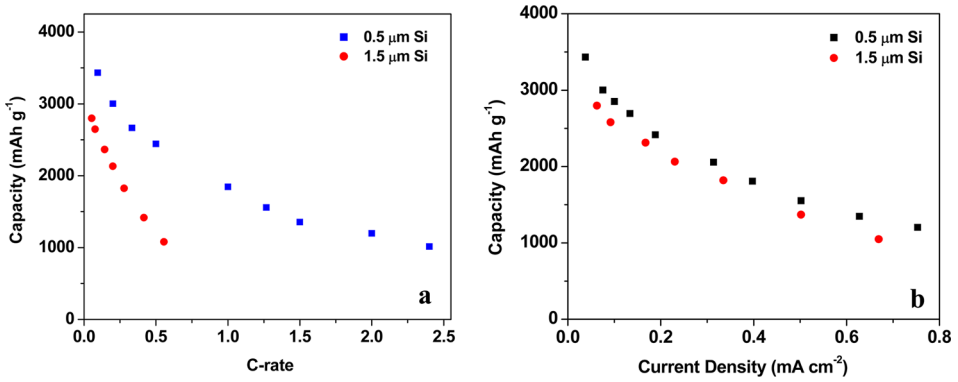

Figure 6. (a) The specific extraction capacities versus the C-rate, (b) specific extraction capacities versus the areal charge−discharge current density of the half-cells: Li | drop-casted gel electrolyte | Si-VACNFs, for the Si thickness of 0.5 and 1.5 μm, respectively.

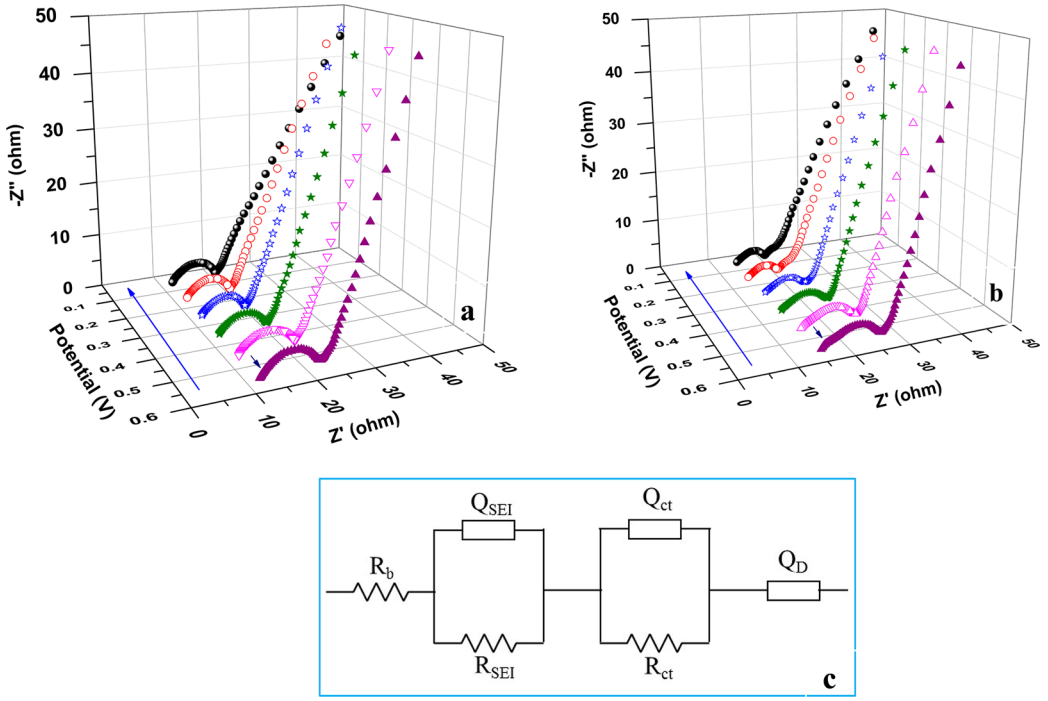

Figure 7. Nyquist plots of the half cell: Li | drop-casted gel electrolyte | Si-VACNFs (Si thickness ~0.5 μm), after (a) 10th cycle and (b) 110th cycle at different static potential from 0.55 to 0.05 V vs Li/Li$^+$. (c) The equivalent circuit used to fit the impedance data.

(Figures S 3d-f), which make it difficult for the gel electrolyte to penetrate down to the bottom of the fibers to form a good interface with all Si surfaces; and (ii) the slow diffusion of Li^+ in Si limited the reaction only in the outer portion of the material at this charge−discharge rate.

For a comparison, half-cells were also fabricated by sandwiching the flexible, self-standing gel films between the Si-coated VACNFs electrode (Si ~ 0.5 μm) and the Li-disc. Figure S8 shows the performance of the cell at different rates varying from a low value of C/11 (0.330 A g^{-1}) to a relatively high value of 1.3C (4.80 A g^{-1}). In the first slow cycle, the insertion capacity was high (3676 mAh g^{-1}) as usual, but the extraction capacity was only 2552 mAh g^{-1}, much lower than the value in liquid electrolytes.[31,32] In the next few cycles, the insertion and extraction capacities became close to each other as the gel infiltrated into Si-VACNFs and stabilized at ~2800 mAh g^{-1} at C/11 rate after 6 cycles. After these initial cycles, the rate performance was evaluated by galvanostatic charge−discharge at different currents from C/11 to as high as 1.3C, each for five cycles, and then followed by a long cycling at C/2.4 (1.6 A g^{-1}) rate (Figure S8). The cell performed fairly well. However, in comparison with the cell fabricated by drop-casting method, the specific capacity was lower at C/11 rate (~2800 mAh g^{-1} vs ~3340 mAh g^{-1}) and dropped more at higher rates (~1200 mAh g^{-1} vs 2342 mAh g^{-1} at ~ C/2). This confirms that the drop-casting method allows the initial fluidic GPE to infiltrate better into the Si-VACNF electrode, which is beneficial for high rate performance and long cycling stability.

The effect of Si thickness on the electrochemical performance with gel polymer electrolyte is further illustrated in Figures 6a and 6b, which compare the specific capacities versus C-rate and areal current density, respectively. As shown in Figure 6a, the half-cells with 0.5 and 1.5 μm nominal Si-thicknesses have specific capacities of ~3450 and 2800 mAh g^{-1} at C/11 rate, respectively. In case of 1.5 μm Si-VACNFs anode, the specific capacity decreases rapidly on increasing the C-rate whereas 0.5 μm Si-VACNFs anode shows relatively high capacity of ~1840 mAh g^{-1} at 1C (or 3.8 A g^{-1}) and ~1000 mAh g^{-1} at 2.4C (9.8

DOI: 10.1021/acsami.5b06444
ACS Appl. Mater. Interfaces 2015, 7, 20909−20918

A g^{-1}). Clearly, the thinner Si coating is fully activated and provides the specific capacity close to the maximum of amorphous Si. In the case of thick Si coating, only a fraction of the exterior silicon is activated in the GPE. The 0.5 μm thick Si-coated VACNFs electrodes have shown excellent electrochemical performance in solid-like GPE, comparable to the reported results of Si-based electrodes in liquid electrolytes.[10,31] Interestingly, the two Si-VACNF electrodes show very similar dependence on the areal current density, as shown in Figure 6b, which further validates that the amount of Si involved in the reaction is similar at any given current. The inner portion of the thick Si shell is not actively used.

It is noteworthy that the vertical structure of the Si-VACNF on Cu foil infiltrated with the GPE is flexible and can be repeatedly bended without irreversible damage. Thus, it has the potential to be used for the development of flexible thin-film rechargeable microbatteries.[28,30] Along this direction, the areal specific capacity is an important metric. For the Si-VACNF with 0.5 μm nominal Si thickness, it is ~0.33 mAh cm^{-2} (~3343 mAh g^{-1}) at C/10.5 rate and ~0.17 mAh cm^{-2} (~1733 mAh g^{-1}) at 1C rate. For the Si-VACNF with 1.5 μm nominal Si thickness, it increases to ~0.84 mAh cm^{-2} (~2800 mAh g^{-1}) at C/11 rate and ~0.37 mAh cm^{-2} (~1200 mAh g^{-1}) at 1C rate. For such applications, a thicker Si coating does have an advantage in boosting up the areal specific capacity due to the larger Si mass loading. Longer VACNFs (up to 20 μm) may be used in future studies to further raise the areal capacity to match the value of ~4 mAh cm^{-2} at C/20 rate in the state-of-the-art flexible LIB anode[30] using 25 μm long Si nanowires. In addition, the mass ratio between carbon (from VACNF) and Si (in the shell) is only ~1:1 in the Si-VACNF with 0.5 μm nominal Si thickness and decreases to only ~1:3 in samples with 1.5 μm nominal Si thickness. Thus, using larger Si thickness may help to reduce the relative mass of the current collectors.

To understand the interface of Si-VACNFs/GPE, electrochemical impedance spectroscopy (EIS) was carried out at various states of charge (SOC) and after varied long cycles. Figure 7, parts a and b, shows the Nyquist plots measured at potentials from 0.55 V (~30% SOC) to 0.05 V (~100% SOC) after the initial 10 cycles at slower rates (initial 2 cycles each at C/10.5 and C/5 rates for cell stabilization and then another 6 cycles at C/10.5 rate) and further 100 cycles at ~1C (3.6 A g^{-1}). Figure 7c depicts the equivalent circuit used to fit the EIS data. The resistance measured at very high frequencies corresponds to the resistance of the GPE (R_b) and is added in series to the circuit. In the high frequency region, the plots consist of two semicircles.[49−51] The first small semicircle represents the contribution of the charge transfer between the gel electrolyte and the SEI (as indicated by the short arrows in the Figure 7, parts a and b) which can be seen more clearly after 110 cycles (Figure 7b). The second semicircle represents the charge transfer between the SEI and the Si anode. In the equivalent circuit (Figure 7c), R_b is the ohmic resistance, R_{SEI} is the charge transfer resistance between the SEI layer and the electrolyte, R_{ct} is the charge transfer resistance between the SEI and Si-VACNFs anode, Q_{SEI} is a constant phase element (CPE) of the SEI, and Q_{ct} is a CPE accounting for the fast pseudocapacitive Li reaction with the active Si shell.[52,53] The low frequency region shows the diffusion behavior of the Li^+ in the Si electrode which cannot be modeled properly by a finite Warburg element.[52,54,55] Here, we replaced the finite diffusion by a CPE (Q_D) which permits us to obtain a good fitting to the experimental data. The admittance response of CPE (Q) can be expressed as follows:

$$\frac{1}{Q} = C\omega^n \cos\left(\frac{n\pi}{2}\right) + jC\omega^n \sin\left(\frac{n\pi}{2}\right) \quad (2)$$

where ω is the angular frequency. A CPE represents a resistor when $n = 0$, a capacitor with capacitance C when $n = 1$, an inductor when $n = -1$, and a Warburg resistance when $n = 0.5$.[52,54] In this study, the CPE appears to be a pseudocapacitor with n lying between 0.5 and 1.

The equivalent circuit model fits all EIS curves very well ($\chi^2 \approx 1 \times 10^{-4}$) and the simulated spectra for some EIS experimental data are compared in Figure S9. The fitting parameters are summarized in Tables S1 and S2. Clearly, R_b is comparable to the measured ohmic resistance of the flexible GPE film and slightly increases after 110 charge−discharge cycles from ~12 Ω to ~15 Ω and unaffected with SOC. The value of R_{SEI} increases from ~1.2 to ~2.1 Ω after 110 cycles which confirms that the formation/deposition of SEI products is a dynamic process varying during the charge−discharge cycles.[32] The value of R_{ct} decreases gradually upon lithiation from 8.89 to 6.83 Ω after 10 cycles and from 9.41 to 6.12 Ω after 110 cycles. Q_D values are very similar in the two sets of data. The small increase in the values of R_b, R_{SEI} and R_{ct} after 100 cycles confirms that the degradation of the GPE is due to its reduction during SEI formation/growth. However, the value of R_b is unchanged during the lithiation of Si-anode (or increasing SOC), which confirms the stability and flexible nature of the GPE. During the volume expansion, the gel is able to accommodate the pressure/stress and the liquid component is not squeezed out of the bulk GPE. Thus, the GPE forms a stable interface with Si-coated VACNFs anode and performs well at high rates and during long cycling. Furthermore, unlike Si-coated VACNFs anode in liquid electrolytes, even the EIS (both before and after long cycles) at 0.05 V did not show the induction loop at low AC frequencies, which served as an indication of a large contribution from SEI formation accompanying lithiation of the Si electrode.[32]

CONCLUSIONS

In this work, the electrochemical performance of the 3D nanostructured Si-VACNF anode in a gel polymer electrolyte is carried out as an effort to develop solid-state lithium-ion batteries. We demonstrated that gel polymer electrolyte can infiltrate into the high-capacity 3D nanostructured anode and form a stable interface. The gel polymer electrolytes shows high conductivity ~2.2 × 10^{-3} S cm^{-1} and sufficient cationic transference number at ambient temperature along with good thermal and mechanical stabilities. The Si-VACNFs/gel electrolyte half-cells have shown high specific capacity, good rate performance, and long cycling stability. By drop-casting the initial fluidic gel polymer electrolyte onto the Si-VACNFs anode, a high capacity of 3450 mAh g^{-1} at C/10.5 (or 0.36 A g^{-1}) rate and 1732 mAh g^{-1} at 1C (or 3.8 A g^{-1}) rate can be obtained. The half-cell also delivers a very high capacity (~1070 mAh g^{-1}) at C/1.5 (or 2.6 A g^{-1}) rate with almost no capacity fade for up to 100 cycles. The electrochemical impedance spectroscopy study confirms that the interface between the Si-VACNFs anode and the gel polymer electrolyte is stable, and the interfacial resistance remains rather constant after 100 cycles at high rates. The excellent rate capability and cycling stability of Si-VACNFs/gel polymer electrolyte cell is attributed

DOI: 10.1021/acsami.5b06444
ACS Appl. Mater. Interfaces 2015, 7, 20909−20918

to the open vertical 3D nanostructure which allows better gel polymer infiltration and provides freedom for Si expansion. The flexible nature of gel polymer electrolyte helps to accommodate the stress/strain during charge−discharge processes. These results show a promising potential for the development of solid-state lithium-ion batteries using the vertical 3D nanostructured electrodes and may be applicable for novel flexible thin-film microbatteries.

■ ASSOCIATED CONTENT

Supporting Information

The Supporting Information is available free of charge on the ACS Publications website at DOI: 10.1021/acsami.5b06444.

Experimental details for conductivity, Li-ion transference number measurements, DSC and TGA studies, DSC/TGA curves, Li-ion transference number measurement curves, SEM images, CV curves, charge−discharge and cycling performance data, EIS fitting curves and fitting parameters. (PDF)

■ AUTHOR INFORMATION

Corresponding Author

*E-mail: junli@ksu.edu.

Notes

The authors declare no competing financial interest.

■ ACKNOWLEDGMENTS

The work at Kansas State University was supported by NSF grant CMMI-1100830, NASA grant NNX13AD42A, NSF EPSCoR Award EPS-0903806, and matching funds provided by the State of Kansas for the latter two. J.W. thanks support by NSF grant number NSF-DMR1508494.

■ REFERENCES

(1) Van Noorden, R. The Rechargeable Revolution: A Better Battery. *Nature* **2014**, *507* (7490), 26−28.

(2) Armand, M.; Tarascon, J.-M. Building Better Batteries. *Nature* **2008**, *451* (7179), 652−657.

(3) Sun, B.; Mindemark, J.; Edström, K.; Brandell, D. Realization of High Performance Polycarbonate-based Li Polymer Batteries. *Electrochem. Commun.* **2015**, *52*, 71−74.

(4) Quartarone, E.; Mustarelli, P. Electrolytes for Solid-State Lithium Rechargeable Batteries: Recent Advances and Perspectives. *Chem. Soc. Rev.* **2011**, *40* (5), 2525−2540.

(5) Agrawal, R. C.; Pandey, G. P. Solid Polymer Electrolytes: Materials Designing and All-Solid-State Battery Applications: An Overview. *J. Phys. D: Appl. Phys.* **2008**, *41* (22), 223001.

(6) Hallinan, D. T., Jr; Balsara, N. P. Polymer Electrolytes. *Annu. Rev. Mater. Res.* **2013**, *43*, 503−525.

(7) Kim, H.-S.; Shin, J.-H.; Moon, S.-I.; Kim, S.-P. Preparation of Gel Polymer Electrolytes using PMMA Interpenetrating Polymeric Network and their Electrochemical Performances. *Electrochim. Acta* **2003**, *48* (11), 1573−1578.

(8) Song, J.; Wang, Y.; Wan, C. Review of Gel-type Polymer Electrolytes for Lithium-ion Batteries. *J. Power Sources* **1999**, *77* (2), 183−197.

(9) Ye, H.; Huang, J.; Xu, J. J.; Khalfan, A.; Greenbaum, S. G. Li Ion Conducting Polymer Gel Electrolytes based on Ionic Liquid/PVDF-HFP Blends. *J. Electrochem. Soc.* **2007**, *154* (11), A1048−A1057.

(10) Chan, C. K.; Peng, H.; Liu, G.; McIlwrath, K.; Zhang, X. F.; Huggins, R. A.; Cui, Y. High-performance Lithium Battery Anodes using Silicon Nanowires. *Nat. Nanotechnol.* **2008**, *3* (1), 31−35.

(11) Park, M.-H.; Kim, M. G.; Joo, J.; Kim, K.; Kim, J.; Ahn, S.; Cui, Y.; Cho, J. Silicon Nanotube Battery Anodes. *Nano Lett.* **2009**, *9* (11), 3844−3847.

(12) Zamfir, M. R.; Nguyen, H. T.; Moyen, E.; Lee, Y. H.; Pribat, D. Silicon Nanowires for Li-based Battery Anodes: A Review. *J. Mater. Chem. A* **2013**, *1* (34), 9566−9586.

(13) Tian, H.; Tan, X.; Xin, F.; Wang, C.; Han, W. Micro-sized Nano-porous Si/C Anodes for Lithium ion Batteries. *Nano Energy* **2015**, *11*, 490−499.

(14) Sun, L.; Wang, X.; Susantyoko, R. A.; Zhang, Q. High Performance Binder-free Sn Coated Carbon Nanotube Array Anode. *Carbon* **2015**, *82*, 282−287.

(15) Chan, C. K.; Zhang, X. F.; Cui, Y. High Capacity Li ion Battery Anodes using Ge Nanowires. *Nano Lett.* **2008**, *8* (1), 307−309.

(16) Szczech, J. R.; Jin, S. Nanostructured Silicon for High Capacity Lithium Battery Anodes. *Energy Environ. Sci.* **2011**, *4* (1), 56−72.

(17) Xu, Y.; Guo, J.; Wang, C. Sponge-like Porous Carbon/Tin Composite Anode Materials for Lithium ion Batteries. *J. Mater. Chem.* **2012**, *22* (19), 9562−9567.

(18) Reyter, D.; Rousselot, S.; Mazouzi, D.; Gauthier, M.; Moreau, P.; Lestriez, B.; Guyomard, D.; Roué, L. An Electrochemically Roughened Cu Current Collector for Si-based Electrode in Li-ion Batteries. *J. Power Sources* **2013**, *239*, 308−314.

(19) Liang, B.; Liu, Y.; Xu, Y. Silicon-based Materials as High Capacity Anodes for Next Generation Lithium ion Batteries. *J. Power Sources* **2014**, *267*, 469−490.

(20) Kasavajjula, U.; Wang, C.; Appleby, A. J. Nano-and Bulk-Silicon-based Insertion Anodes for Lithium-ion Secondary Cells. *J. Power Sources* **2007**, *163* (2), 1003−1039.

(21) Yao, Y.; McDowell, M. T.; Ryu, I.; Wu, H.; Liu, N.; Hu, L.; Nix, W. D.; Cui, Y. Interconnected Silicon Hollow Nanospheres for Lithium-ion Battery Anodes with Long Cycle Life. *Nano Lett.* **2011**, *11* (7), 2949−2954.

(22) Liu, N.; Wu, H.; McDowell, M. T.; Yao, Y.; Wang, C.; Cui, Y. A Yolk-shell Design for Stabilized and Scalable Li-ion Battery Alloy Anodes. *Nano Lett.* **2012**, *12* (6), 3315−3321.

(23) Terranova, M. L.; Orlanducci, S.; Tamburri, E.; Guglielmotti, V.; Rossi, M. Si/C Hybrid Nanostructures for Li-ion Anodes: An Overview. *J. Power Sources* **2014**, *246*, 167−177.

(24) Cui, L.-F.; Yang, Y.; Hsu, C.-M.; Cui, Y. Carbon-silicon Core-shell Nanowires as High Capacity Electrode for Lithium ion Batteries. *Nano Lett.* **2009**, *9* (9), 3370−3374.

(25) Wang, W.; Epur, R.; Kumta, P. N. Vertically Aligned Silicon/Carbon Nanotube (VASCNT) Arrays: Hierarchical Anodes for Lithium-ion Battery. *Electrochem. Commun.* **2011**, *13* (5), 429−432.

(26) Gohier, A.; Laïk, B.; Kim, K. H.; Maurice, J. L.; Pereira-Ramos, J. P.; Cojocaru, C. S.; Van, P. T. High-Rate Capability Silicon Decorated Vertically Aligned Carbon Nanotubes for Li-ion Batteries. *Adv. Mater.* **2012**, *24* (19), 2592−2597.

(27) Fan, Y.; Zhang, Q.; Xiao, Q.; Wang, X.; Huang, K. High Performance Lithium ion Battery Anodes Based on Carbon Nanotube-silicon Core−shell Nanowires with Controlled Morphology. *Carbon* **2013**, *59*, 264−269.

(28) Gwon, H.; Hong, J.; Kim, H.; Seo, D.-H.; Jeon, S.; Kang, K. Recent Progress on Flexible Lithium Rechargeable Batteries. *Energy Environ. Sci.* **2014**, *7* (2), 538−551.

(29) Kil, E. H.; Choi, K. H.; Ha, H. J.; Xu, S.; Rogers, J. A.; Kim, M. R.; Lee, Y. G.; Kim, K. M.; Cho, K. Y.; Lee, S. Y. Imprintable, Bendable, and Shape-Conformable Polymer Electrolytes for Versatile-Shaped Lithium-ion Batteries. *Adv. Mater.* **2013**, *25* (10), 1395−1400.

(30) Vlad, A.; Reddy, A. L. M.; Ajayan, A.; Singh, N.; Gohy, J.-F.; Melinte, S.; Ajayan, P. M. Roll up Nanowire Battery from Silicon Chips. *Proc. Natl. Acad. Sci. U. S. A.* **2012**, *109* (38), 15168−15173.

(31) Klankowski, S. A.; Rojeski, R. A.; Cruden, B. A.; Liu, J.; Wu, J.; Li, J. A High-performance Lithium-ion Battery Anode Based on the Core-shell Heterostructure of Silicon-coated Vertically Aligned Carbon Nanofibers. *J. Mater. Chem. A* **2013**, *1* (4), 1055−1064.

(32) Klankowski, S. A.; Pandey, G. P.; Cruden, B. A.; Liu, J.; Wu, J.; Rojeski, R. A.; Li, J. Anomalous Capacity Increase at High-rates in

DOI: 10.1021/acsami.5b06444
ACS Appl. Mater. Interfaces 2015, 7, 20909−20918

Lithium-ion Battery Anodes Based on Silicon-coated Vertically Aligned Carbon Nanofibers. *J. Power Sources* **2015**, *276*, 73−79.
(33) Pandey, G. P.; Agrawal, R. C.; Hashmi, S. A. Magnesium Ion-conducting Gel Polymer Electrolytes Dispersed with Nanosized Magnesium Oxide. *J. Power Sources* **2009**, *190* (2), 563−572.
(34) Cruden, B. A.; Cassell, A. M.; Ye, Q.; Meyyappan, M. Reactor Design Considerations in the Hot Filament/Direct Current Plasma Synthesis of Carbon Nanofibers. *J. Appl. Phys.* **2003**, *94* (6), 4070−4078.
(35) Melechko, A. V.; Merkulov, V. I.; McKnight, T. E.; Guillorn, M.; Klein, K. L.; Lowndes, D. H.; Simpson, M. L. Vertically Aligned Carbon Nanofibers and Related Structures: Controlled Synthesis and Directed Assembly. *J. Appl. Phys.* **2005**, *97* (4), 041301.
(36) Liu, J.; Essner, J.; Li, J. Hybrid Supercapacitor Based on Coaxially Coated Manganese Oxide on Vertically Aligned Carbon Nanofiber Arrays. *Chem. Mater.* **2010**, *22* (17), 5022−5030.
(37) Bamford, D.; Reiche, A.; Dlubek, G.; Alloin, F.; Sanchez, J.-Y.; Alam, M. Ionic Conductivity, Glass Transition, and Local Free Volume in Poly(ethylene oxide) Electrolytes: Single and Mixed ion Conductors. *J. Chem. Phys.* **2003**, *118* (20), 9420−9432.
(38) Zhao, J.; Wang, L.; He, X.; Wan, C.; Jiang, C. Determination of Lithium-Ion Transference Numbers in $LiPF_6$-PC Solutions Based on Electrochemical Polarization and NMR Measurements. *J. Electrochem. Soc.* **2008**, *155* (4), A292−A296.
(39) Zugmann, S.; Fleischmann, M.; Amereller, M.; Gschwind, R. M.; Wiemhöfer, H.; Gores, H. Measurement of Transference Numbers for Lithium Ion Electrolytes via Four Different Methods, a Comparative Study. *Electrochim. Acta* **2011**, *56* (11), 3926−3933.
(40) Zhu, Y.; Wang, F.; Liu, L.; Xiao, S.; Chang, Z.; Wu, Y. Composite of a Nonwoven Fabric with Poly (vinylidene fluoride) as a Gel Membrane of High Safety for Lithium Ion Battery. *Energy Environ. Sci.* **2013**, *6* (2), 618−624.
(41) Klankowski, S. A.; Pandey, G. P.; Malek, G. A.; Wu, J.; Rojeski, R. A.; Li, J. A Novel High-Power Battery-Pseudocapacitor Hybrid Based on Fast Lithium Reactions in Silicon Anode and Titanium Dioxide Cathode Coated on Vertically Aligned Carbon Nanofibers. *Electrochim. Acta* **2015**, *178*, 797.
(42) Polat, B. D.; Eryılmaz, O. L.; Chen, Z.; Keles, O.; Amine, K. High Capacity Anode with Well-aligned, Ordered NiSi Nano-columnar Arrays. *Nano Energy* **2015**, *13*, 781−789.
(43) Hassan, F. M.; Chabot, V.; Elsayed, A. R.; Xiao, X.; Chen, Z. Engineered Si Electrode Nanoarchitecture: A Scalable Postfabrication Treatment for the Production of Next-generation Li-ion Batteries. *Nano Lett.* **2013**, *14* (1), 277−283.
(44) McSweeney, W.; Lotty, O.; Glynn, C.; Geaney, H.; Holmes, J.; O'Dwyer, C. The Influence of Carrier Density and Doping Type on Lithium Insertion and Extraction Processes at Silicon Surfaces. *Electrochim. Acta* **2014**, *135*, 356−367.
(45) Chan, C. K.; Ruffo, R.; Hong, S. S.; Cui, Y. Surface Chemistry and Morphology of the Solid Electrolyte Interphase on Silicon Nanowire Lithium-ion Battery Anodes. *J. Power Sources* **2009**, *189* (2), 1132−1140.
(46) Xiao, Q.; Fan, Y.; Wang, X.; Susantyoko, R. A.; Zhang, Q. A Multilayer Si/CNT Coaxial Nanofiber LIB Anode with a High Areal Capacity. *Energy Environ. Sci.* **2014**, *7* (2), 655−661.
(47) Netz, A.; Huggins, R. A.; Weppner, W. The Formation and Properties of Amorphous Silicon as Negative Electrode Reactant in Lithium Systems. *J. Power Sources* **2003**, *119*, 95−100.
(48) Hatchard, T.; Dahn, J. In situ XRD and Electrochemical Study of the Reaction of Lithium with Amorphous Silicon. *J. Electrochem. Soc.* **2004**, *151* (6), A838−A842.
(49) Lin, Y.-M.; Lkavetter, K.; Abel, P.; Davy, N.; Snider, J.; Heller, A.; Mullins, C. High Performance Silicon Nanoparticle Anode in Fluoroethylene Carbonate-based Electrolyte for Li-ion Batteries. *Chem. Commun.* **2012**, *48* (58), 7268−7270.
(50) Wang, H.-Y.; Wang, F.-M. Electrochemical Investigation of an Artificial Solid Electrolyte Interface for Improving the Cycle-ability of Lithium ion Batteries using an Atomic Layer Deposition on a Graphite Electrode. *J. Power Sources* **2013**, *233*, 1−5.
(51) Hang, T.; Mukoyama, D.; Nara, H.; Yokoshima, T.; Momma, T.; Li, M.; Osaka, T. Electrochemical Impedance Analysis of Electrodeposited Si−O−C Composite Thick Film on Cu Micro-cones-arrayed Current Collector for Lithium Ion Battery Anode. *J. Power Sources* **2014**, *256*, 226−232.
(52) Zhang, S.; Shi, P. Electrochemical Impedance Study of Lithium Intercalation into MCMB Electrode in a Gel Electrolyte. *Electrochim. Acta* **2004**, *49* (9), 1475−1482.
(53) Qian, X.; Gu, N.; Cheng, Z.; Yang, X.; Wang, E.; Dong, S. Plasticizer Effect on the Ionic Conductivity of PEO-based Polymer Electrolyte. *Mater. Chem. Phys.* **2002**, *74* (1), 98−103.
(54) Kim, Y.-O.; Park, S.-M. Intercalation Mechanism of Lithium Ions into Graphite Layers Studied by Nuclear Magnetic Resonance and Impedance Experiments. *J. Electrochem. Soc.* **2001**, *148* (3), A194−A199.
(55) Wang, C.; Appleby, A. J.; Little, F. E. Electrochemical Impedance Study of Initial Lithium ion Intercalation into Graphite Powders. *Electrochim. Acta* **2001**, *46* (12), 1793−1813.

DOI: 10.1021/acsami.5b06444
ACS Appl. Mater. Interfaces 2015, 7, 20909−20918